Glycogen synthase kinase 3 activity enhances liver inflammation in MASH

Mireille Khoury, Qianqian Guo, Kunimaro Furuta, Cristina Correia, Chady Meroueh, Hyun Se Kim Lee, Khaled Warasnhe, Lucía Valenzuela Pérez, Andrew P. Mazar, Iljung Kim, Yung-Kyun Noh, Heather Holmes, Michael F. Romero, Caroline R. Sussman, Kevin D. Pavelko, Shahidul Islam, Adebowale O. Bamidele, Petra Hirsova, Hu Li, Samar H. Ibrahim

Table of contents

Materials and methods

Materials. Palmitate (PA) (P0500) was obtained from Sigma-Aldrich (St. Louis, MO, USA). Louis, MO). Primary antibodies employed for the studies include anti-alpha smooth muscle actin (α-SMA) (ab124964) from Abcam (Cambridge, MA), anti-GAPDH (MAB374) from Millipore Sigma, anti-β-actin (sc-47778) from Santa Cruz Biotechnologies (Santa Cruz, CA), anti-H/M Myeloperoxidase (MPO) (#AF3667), anti-ICAM-1 (#AF796SP) from R&D systems, anti-GSK3β (D5C5Z) (#12456), anti-phospho-β-catenin (Ser33/37/Thr41) (#9561), anti-glycogen synthase (3893S), anti-phospho glycogen synthase (Ser641) (#3891S), anti-VE-Cadherin (#2158S), anti-FAK (#3285S) and anti F4/80 (#70076S) from Cell Signaling Technology (Danvers, MA), and anti-phospo-GSK3α/β (Try216/Try279) (#44-604G), anti-phospho FAK (#44-624G), anti-phospho VE-Cadherin (Tyr658) (#44-1144G) from Thermo Fisher Scientific (Waltham, MA). Recombinant human TNF-α (210-TA) and TGF-β1 (7754-BH) were obtained from R&D Systems. LY2090314 (S7063) was purchased from Selleck Chemicals, LLC (Houston, TX, USA). Elraglusib (9-ING-41) was gifted by Acuate Therapeutics Inc. (Fort Worth, TX, USA).

Cells. Primary human liver sinusoidal endothelial cells (LSEC) were purchased from ScienCell Research Laboratories (San Diego, CA). Primary mouse LSEC were isolated using collagenase perfusion and immunomagnetic selection as previously described[1, 2]. Briefly, the liver was digested with collagenase infused via the portal vein, and the obtained cell suspensions were centrifuged at 50 × g for 2 min to remove the hepatocytes. The supernatant, which included non-parenchymal cells, was subjected to LSEC isolation using CD146 MicroBeads (Miltenyi Biotec, Bergisch Gladbach, Germany) following the manufacturer's instructions. Primary human and mouse LSEC and immortalized mouse LSEC cell lines (TSEC) were cultured in Endothelial Cell Growth Medium (211-500, Sigma) consisting of 5% fetal bovine serum (FBS) and 1% endothelial

cell growth supplement supplemented with 1% primocin (InvivoGen, San Diego, CA). TSEC were generated by Dr. Shah's lab from LSEC isolated from mouse liver using CD31-based immunomagnetic separation, immortalized with SV40 large T-antigen, and subcloned based on their ability to endocytose acetylated low-density lipoprotein. The resulting cell line, transformed sinusoidal endothelial cells (TSEC), maintains an endothelial phenotype as well as some LSEC-specific features [3]. The human monocytic cell line THP-1, derived from a 1-year-old boy with acute monocytic leukemia, was purchased from ATCC (Rockville, MD, USA) and cultured in RPMI-1640 medium supplemented with 10% fetal bovine serum. All the cell cultures were maintained at 37°C in a humidified atmosphere containing 5% CO_2. GSK3β knockdown in LSEC was performed using siRNA. Primary human LSEC were transfected with either Accell human siGSK3b smart pool or a non-target control siRNA (NT) (Horizon Discovery/Dharmacon, Cambridge, UK) and cultured for 72 h, followed by treatment with either vehicle or 500μM PA. Knock-down efficacy was assessed by western blotting or qPCR for GSK3β.

Immunoblot analysis. Deidentified human liver tissues obtained by liver biopsy or surgical hepatic resection from patients with normal livers, isolated steatosis, or MASH were acquired (Institutional Review Board (IRB) #22-000320) and homogenized in T-PER lysis buffer (#78510, Roche) containing protease and phosphatase inhibitors (#78442, Thermo Scientific). Cells were lysed using RIPA buffer (50 mM Tris-HCl, pH 7.4; 1% Nonidet P-40; 0.25% sodium deoxycholate; 150 mM NaCl; 1 mM EDTA with protease inhibitors), followed by centrifugation at 15,000 × g for 15 min at 4°C. Protein concentrations in the lysates were measured using the Bradford assay (Sigma-Aldrich). Equal amounts of protein were loaded onto sodium dodecyl sulfate (SDS)-sulfate-polyacrylamide gel electrophoresis (PAGE) gels, transferred to nitrocellulose membranes (Bio-Rad, Hercules, CA, USA), and incubated overnight with the

primary antibody of interest. All primary antibodies were used at a dilution of 1:1,000 unless otherwise recommended by the manufacturer. Horseradish peroxidase-conjugated secondary antibodies against rabbit (Alpha Diagnostic International, San Antonio, TX, USA) or mouse (Southern Biotech, Birmingham, AL, USA) were used at a dilution of 1:5,000 and incubated for 1 h at room temperature. The proteins were detected using enhanced chemiluminescence reagents (GE Healthcare, Chicago, IL, USA). β-actin and GAPDH protein levels were used as loading controls.

Transendothelial Migration (TEM) Assay. As previously described[4, 5], we conducted a monocyte transendothelial assay using a hydrated collagen gel (PureCol Type I collagen solution, Advanced BioMatrix, 5005) culture system. Primary human LSEC (100 μl of 0.5×10^6 cells/ml) were labeled with Vybrant DiI solution (Molecular Probes, MP22885) and plated on hydrated collagen gel in each well of a 96-well plate to form a monolayer and then treated with vehicle or PA with or without the GSK3 inhibitor LY2090314 at a concentration of 20 μM for 16 h. The human monocytic cell line THP-1 (100 μl of 0.5×10^6 cells/ml) was labeled with Vybrant DiO solution (Molecular Probes, MP22885) and added to each well of a confluent human LSEC monolayer grown on top of the hydrated collagen gels. THP-1 cells were allowed to migrate for 1 h at 37°C and 5% CO_2. The monolayers were washed 3 times with warm DPBS/RPMI (200 μl per wash) to remove unattached monocytes. Monolayers were then fixed and imaged, and monocyte transmigration was quantified by confocal microscopy (Zeiss, LSM-780).

Migration assay. Bone marrow-derived monocytes were isolated from C57BL/6J mice (Jackson Laboratory). Briefly, bone marrow was extracted from dissected mouse tibia and femur, and monocytes were isolated using a Monocyte Isolation Kit (#130-100-629, Miltenyi Biotech) as described by the manufacturer. The cells were resuspended in RPMI-1640 medium without

phenol red (#11835030, Gibco) and fluorescently labeled with CellTracker Red CMTPX (#C34552, Invitrogen). Cells were treated for 30 min with vehicle (dimethyl sulfoxide), GSK3 inhibitors (LY 100 nM or ING 1 μM), or cenicriviroc (1 μM, #HY-14882A, MedChemExpress) in transwell inserts (5 μm pores, #3421, Corning) placed in a 24-well plate. RPMI medium with or without 100 ng/ml recombinant murine CCL2 (#250-10, PeproTech) was loaded into the bottom of the lower chamber of the 24-well plate. Cells were allowed to migrate for 3 h, after which the migrated cells in the lower chamber were counted using an automated plate-based imaging cytometer (Nexcelom Celigo S Imaging Cytometer).

Flow-based adhesion assay. Primary neutrophils were isolated from whole blood drawn from healthy adult volunteers (Institutional Review Board (IRB) #22-000320) using a human neutrophil isolation kit following the manufacturer's instructions (130-104-434, Miltenyi Biotec, Germany) and used within 4 h of isolation. Primary human LSEC were cultured in a collagen-coated Ibidi μ-Slide I Luer 0.4 (Cat #80176, Ibidi, Germany), and pre-treated with the GSK3 inhibitor LY2090314 (LY) 20 nM for two hours, then treated with PA 500 μM with or without LY overnight. A perfusion system with endothelial basal medium was connected and a shear flow of 0.8 dyne/cm^2 was applied. Freshly isolated neutrophils were incubated at 37°C for 30 min before being injected into the perfusion system. We then flushed 1.7 x 10^6 neutrophils per condition through the LSEC monolayer for 30 min, and non-adherent neutrophils were washed away by flushing the slide with basal medium for 20 min. Primary mouse LSEC were isolated as previously described [2]. A similar adhesion assay was performed to evaluate adhesion of primary mouse monocytes to primary mouse LSECs. Monocytes were isolated from healthy mice, and LSECs were isolated from either chow-fed vehicle-treated or CDHFD diet fed vehicle/9-ING-41 treated

mice as described previously. Bright-field images were taken, and adherent and transmigrated neutrophils or monocytes were counted using the Fiji software.

Animals. The study protocols were approved by the Institutional Animal Care and Use Committee (IACUC) of the Mayo Clinic. The methods employed in the current study were conducted according to the IACUC guidelines for the use of anesthetics in experimental mice. Mice were housed and bred in a temperature-controlled 12:12-hour light-dark cycle facility with free access to food. All interventions were performed during the light cycle. C57BL/6J mice were purchased from Jackson Laboratory (Bar Harbor, ME, USA).

Diet-induced Murine NASH Models. Eight-week-old C57BL/6J wild-type (WT) mice were fed either a chow diet (5053 PicoLab Rodent Diet 20; LabDiet, St. Louis, MO, USA) or a diet rich in fat, fructose, and cholesterol (FFC), starting at the age of 8-weeks for 24 weeks. The FFC diet consisted of 40% energy as fat (12% saturated fatty acid, 0.2% cholesterol) (AIN-76A Western Diet, TestDiet, St Louis, MO), with fructose (23.1 g/L), and glucose (18.9 g/L) in drinking water. The FFC diet-induced metabolic dysfunction associated with steatohepatitis (MASH) phenocopies the human disease and associated metabolic syndrome[6] and has been well validated by us[7, 8]. At 20 weeks on the diet, the mice were randomized to receive either vehicle or the GSK3 inhibitor LY2090314 intraperitoneally at 10 mg/kg body weight/dose 3 times a week for the last 4 weeks of the study. The dose employed was optimized based on a previously published study in a different disease model[9] and a pilot study in FFC-fed mice with dose modification to maintain tolerance. In an independent study, Eight-week-old C57BL/6J WT mice were fed a choline-deficient high-fat diet (CDHFD) (A06071302, Research Diet), which consists of 60% fat, 0.1% methionine, and no added choline, starting at 8 weeks of age for 6 weeks. Mice fed the CDHFD experienced minimal body weight loss as opposed to those fed the traditional methionine and choline-deficient

diet and had hepatic steatosis, ALT elevation, hepatocyte ballooning, hepatic inflammation, and fibrosis, recapitulating the histological features of human NASH, as shown in previous studies[1, 10]. Elraglusib (9-ING-41) was gifted by Acuate Therapeutics Inc. (Fort, Worth, TX), the dose employed was 30 mg/kg/day IP for 2 weeks during the last 2 weeks of the feeding study, was based on extensive pharmacodynamic and pharmacokinetic profiling by the company, and was the same dose employed in a different disease model[11].

Assessment of metabolic profiles in mice. At the 3rd week of LY treatment, total caloric intake was calculated based on the weight of food and drinking water consumption. Metabolic parameters, including oxygen consumption, carbon dioxide production, and respiratory exchange ratio, were measured using a comprehensive laboratory animal monitoring system (CLAMS; Columbus Instruments, OH, USA). These calorimetry chambers were also equipped with sensors that allowed the measurement of physical activity. Lean verus fat body composition was measured using echo-MRI. Blood glucose and plasma insulin levels were measured using Assure 4 (Arkray, Edina, MN) and Ultra-Sensitive Mouse Insulin enzyme-linked immunosorbent assay (ELISA) kits (Crystal Chem Inc., Downers Grove, IL), respectively. The homeostasis model assessment of insulin resistance (HOMA-IR) was calculated using the following formula: HOMA-IR = 26 × fasting insulin level (ng/mL) × fasting glucose level (mg/dL)/405[1].

Measurement of liver triglyceride and alanine aminotransferase levels. Liver triglyceride (TG) levels were measured in the mouse liver homogenates. Fifty milligrams of liver tissue were homogenized in a 5% NP-40 solution. The EnzyChrom Triglyceride Kit (BioAssay System, CA, USA) was used according to the manufacturer's instructions. The photometric absorbance was read at 570 nm using a Synergy H1 microplate reader (BioTek). Serum alanine aminotransferase

(ALT) levels were measured using VetScan2 (Abaxis Veterinary Diagnostics, Union City, CA, USA).

Histological, immunohistochemical, and digital imaging analyses. Hematoxylin and eosin (H&E) and Sirius red staining were performed as previously described[12]. Histology was assessed using the non-alcoholic fatty liver disease (NAFLD) activity score (NAS), a semi-quantitative score that accounts for steatosis, ballooned hepatocytes, and lobular inflammation[13]. Sirius red-stained tissue was imaged using red fluorescence and individual collagen fibers were automatically detected and quantified for width, length, and straightness using CT-FIRE [14, 15]. The tissue area was determined using ImageJ software. Formalin-fixed paraffin-embedded mouse liver tissue sections were deparaffinized, hydrated, and stained with antibodies against F4/80 (1:500), ICAM-1 (1:2,000), MPO (1:1,000), or α-SMA (1:1,000). The bound antibody was detected using a Vectastain ABC kit for goat (PK-6105 or PK-6101, Vector Laboratories, Burlingame, CA) and DAB substrate (Vector Laboratories) according to the manufacturer's instructions. Tissue sections were counterstained with hematoxylin. MPO staining was evaluated by immunofluorescence with an anti-goat alexa-568 secondary antibody (#A-11057, Thermo Fisher Scientific). Liver injury was assessed by the number of apoptotic hepatocytes using the terminal deoxynucleotidyl transferase deoxyuridine triphosphate nick-end labeling (TUNEL) assay and an In Situ Cell Death Detection Kit (Roche) following the manufacturer's instructions. The H&E-stained slides and ICAM1-stained slides were scanned using an Aperio AT2 scanner (Leica Biosystems) at 20X magnification at the pathology research core at the Mayo Clinic. The slides were annotated by a liver pathologist using Qupath 0.4 [14] for the central vein (CV) and portal vessel (PV) locations. The whole-slide images were then analyzed using a nonparametric supervised machine learning method through a Gaussian Process

(GP). A nonlinear boundary between different zones was acquired using nonlinear regression, showing the anatomical distance to the boundary annotations of both the CV and PV. A Gaussian process (GP) regression was used to predict the target value of-1 on the CV boundary contours and +1 on the PV boundary. A topographic map was constructed with three boundaries between zones determined by the level curve, with a GP output of -0.5 and +0.5. The whole slide images with the 3-zones contour were then analyzed using Qupath for ICAM-1 staining positivity surface area in each zone through an OpenCV pixel classifier using the diaminobenzidine (DAB) channel with a fixed threshold of 0.6 and a Gaussian prefilter at 1. The results included quantification of the ICAM-1 positive area within each zone. Steatosis quantification was performed using a machine learning algorithm trained on human liver biopsies [16].

Ultrasound-Based Liver Elastography. The mice were anesthetized with inhaled isoflurane (2-3%), shaved, and depilated. The mice were placed in the supine position on an imaging platform with the temperature maintained at 37 °C. We employed high-frequency (22 MHz) ultrasound using a Vega system (SonoVol) to image the mice. The transducer was moved to the liver and the region of interest (ROI) was adjusted to include only liver tissue. Six consecutive 2D shear wave elastography (SWE) scans were taken at 0.5 mm intervals through the liver. The median Young's Modulus for the ROI for each scan was calculated using SonoEQ software (SonoVol) and then averaged for each animal. One-way ANOVA was used for statistical analysis of significance.

Tandem Mass Tag (TMT)-based on quantitative total and phospho-proteomics. As previously described, LSEC isolated from FFC-fed NASH or chow-fed control mice were subjected to liquid chromatography-mass spectrometry (LC-MS) sample preparation. [17] One hundred micrograms of protein from each sample was TCA-precipitated. After washing with acetone and methanol, the protein pellet was reconstituted in 100 µl of 200 mM HEPES (pH 8.5). The samples were digested

with Lys-C overnight at room temperature and then trypsinized for 6 h at 37°C at a 1:100 protease-to-protein ratio. To each digest 234, µg of TMTpro16plex reagents (12 µl) and 30 µl of 100% anhydrous acetonitrile were added for labeling (labels used: 126:293T Vehicle (V); 127N: 293T Torin1 (T); 127C: RPE1 V; 128N: RPE1 T; 128C: U2OS V; 129N: U2OS T; 129C: HeLa V; 130N: HeLa T; 130C: MCF7 V; 131N: MCF7 T; 131C: HCT116 V; 132N: HCT116 T; 132C: Panc1 V; 133N: Panc1 T; 133C: RKO V; 134N: RKO T). The samples were then labeled for 60 min at room temperature. Two microliters (1.4% v/v) of each sample was pooled, desalted, and analyzed by MS to check the labeling efficiency. After checking the labeling efficiency, the samples were quenched by adding 5 µl of 5% hydroxylamine and pooled. The pooled samples were desalted using 200 mg Sep-Pak solid-phase extraction columns. A Pierce High-Select Fe-NTA phosphopeptide enrichment kit was used to enrich phosphopeptides from the pooled mixture. The unbound fraction and column washes were combined, desalted, and fractionated by bRPLC. Fractions were collected in a 96-well plate and combined for a total of 24 fractions (A and B sets) before desalting and subsequent LC–MS/MS analysis.

Integrated omics analysis. Differentially expressed genes (p-value < 0.05) between chow-fed mice and FFC-fed mice in the LSEC total proteomic analysis or our previous LSEC transcriptomic analysis (GSE164006)[1]) were subjected to Kyoto Encyclopedia of Genes and Genomes (KEGG) overrepresentation pathway analysis. The mass spectrometry proteomics data were deposited in the ProteomeXchange Consortium via the PRIDE [18] partner repository with the dataset identifier PXD048073.

Nanostring-based gene expression profiling. The gene expression profile of HHSECs was assessed using a NanoString nCounter system (NanoString Technologies, Seattle, WA, USA). We employed the Human Fibrosis V2 panel, in which 760 fibrosis-related human genes and 10

housekeeping reference genes were implemented. All procedures, including sample preparation (100 ng of RNA per sample), hybridization (at 65°C for 17 h), detection, and subsequent analysis, were performed according to the manufacturer's instructions. After quality control and background thresholding using built-in negative control probes, the data were normalized to the positive hybridization controls and housekeeping genes.

Quantitative reverse transcription PCR (qRT-PCR). Total RNA was isolated using the RNeasy Mini Kit (Qiagen, Valencia, CA, USA) and reverse-transcribed with Moloney murine leukemia virus reverse transcriptase and oligo-dT random primers (both from Invitrogen, CA, USA). Gene expression was quantified by real-time PCR using SYBR green fluorescence on a LightCycler 480 instrument (Roche Applied, IN, USA) **(primers are listed in Supplementary Table 4)**. The target gene expression was calculated and normalized using the ΔΔCt method.

Mass Cytometry by time-of-flight (CyTOF) analysis. Four random mice from each cohort were selected for intrahepatic leukocyte isolation by using a liver dissociation kit and Percoll gradient centrifugation. Cells were suspended in Maxpar Cell Staining Buffer (CSB) (Fluidigm, San Francisco, CA) and labeled with 0.5 μM cisplatin (Fluidigm) solution. After centrifugation, the cells were resuspended in CSB before addition of the cell surface antibody staining cocktail in an equal volume of CSB. Cells were incubated with gentle agitation at room temperature for 45 min. Following a wash with CSB, samples were permeabilized with eBioscience FoxP3/Transcription factor/fixation/permeabilization solution (Thermo Fisher, Waltham, MA), washed, and resuspended in permeabilization buffer before the addition of the intracellular antibody staining cocktail. Cells were incubated at room temperature for 45 min with gentle agitation. Following washing with PBS, the cells were fixed with 2% paraformaldehyde using gentle agitation at 4°C for 30 min. Cells were washed with CSB and DNA intercalation was performed by adding 1:10000

diluted 125 μM of Cell ID™ Intercalator-Ir (Fluidigm) with gentle agitation at 4°C overnight. Cells were resuspended in a 1:10 dilution of EQ beads (EQ Four Element Calibration Beads, Fluidigm) and then loaded onto the Helios sample loader for data acquisition. Mass cytometry was performed in the Immune Monitoring Core at the Mayo Clinic, and antibodies conjugated to stable heavy metal isotopes were employed to detect cellular antigens by mass cytometry time-of-flight (CyTOF) and enable comprehensive profiling of the phenotype and function of intrahepatic leukocytes. After data acquisition, fcs files were normalized using CyTOF Software (version 6.7.1014). Cleanup of cell debris, removal of doublets, and dead cells were performed using FlowJo software version 10.5.3 (Ashland, OR). The cleaned fcs files were analyzed using the R-based tool CyTOF kit version 3.8[19]. Clustering and dimensionality reduction to 20,000 events per file were performed using the Rphenograph algorithm, which included 32 different cell surface markers and two cytosolic markers (S100A8 and MPO) in the panel **(Supplementary Table 1-3, Fig. S8)**. Visualization of the clusters was performed using a tSNE map. Relative marker intensities and cluster abundances per sample were visualized using a heat map.

Statistical analysis. Data are expressed as mean ± SEM. Differences between multiple groups were compared using one-way analysis of variance followed by Bonferroni's multiple comparisons test or Student's t-test when comparing two groups. *, **, ***, **** indicate statistical significance with $p < 0.05$, $p < 0.01$, $p < 0.001$ and $p < 0.0001$, respectively. Statistically non-significant results are labeled as ns, where appropriate. All analyses were performed using the GraphPad Prism 9.2.0 software (CA, USA).

Supplementary figures

Fig. S1

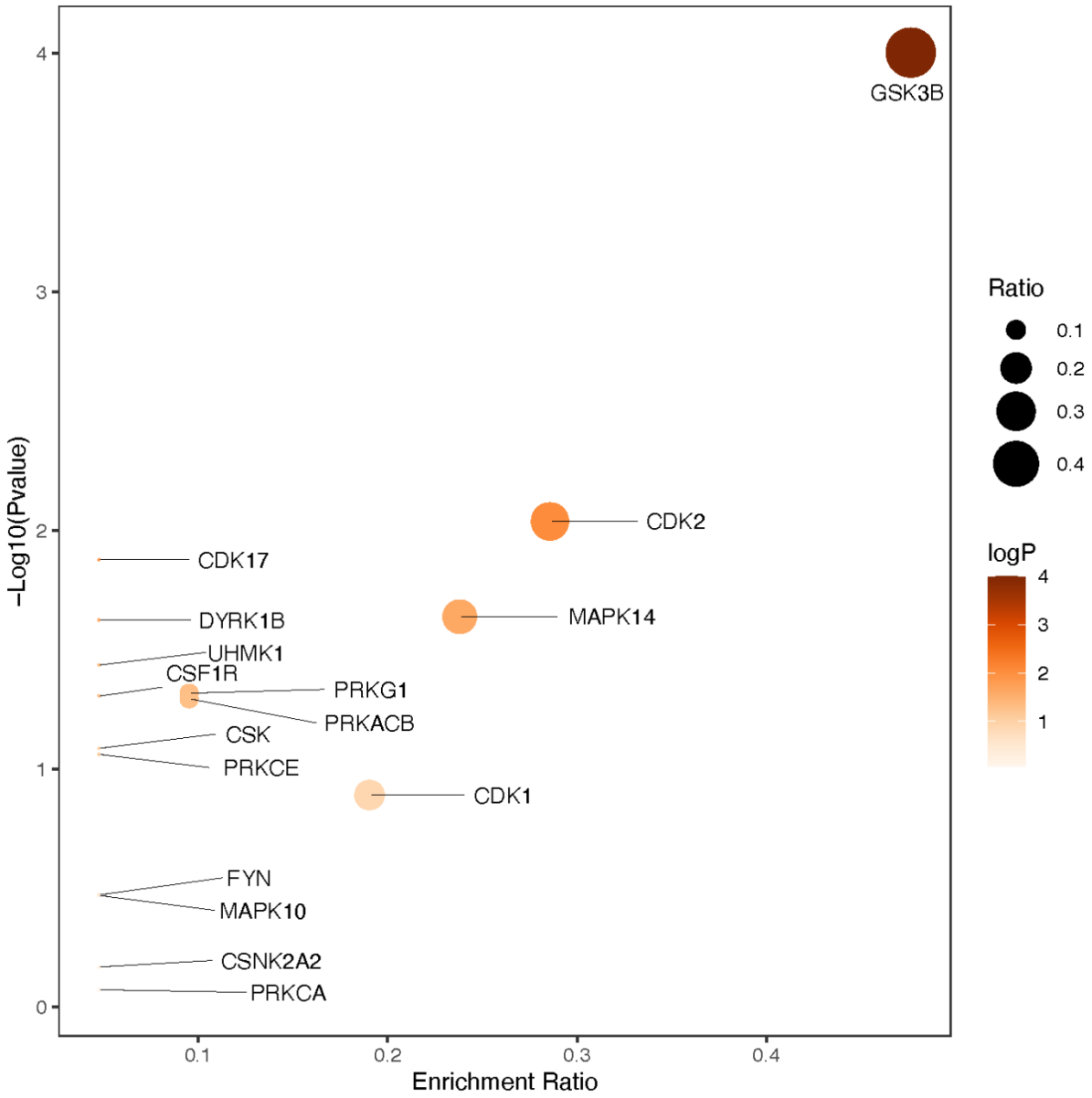

Fig. S1. GSK3β is the top hub kinase altered in the MASH LSEC. Enrichment ratio (bubble size) and log (p-value) values for the top 16 ranked putative altered kinases in FFC versus chow-fed mice generated from the phospho-proteomic study are shown in **(Figure 1A).**

Supplemental Figure 2

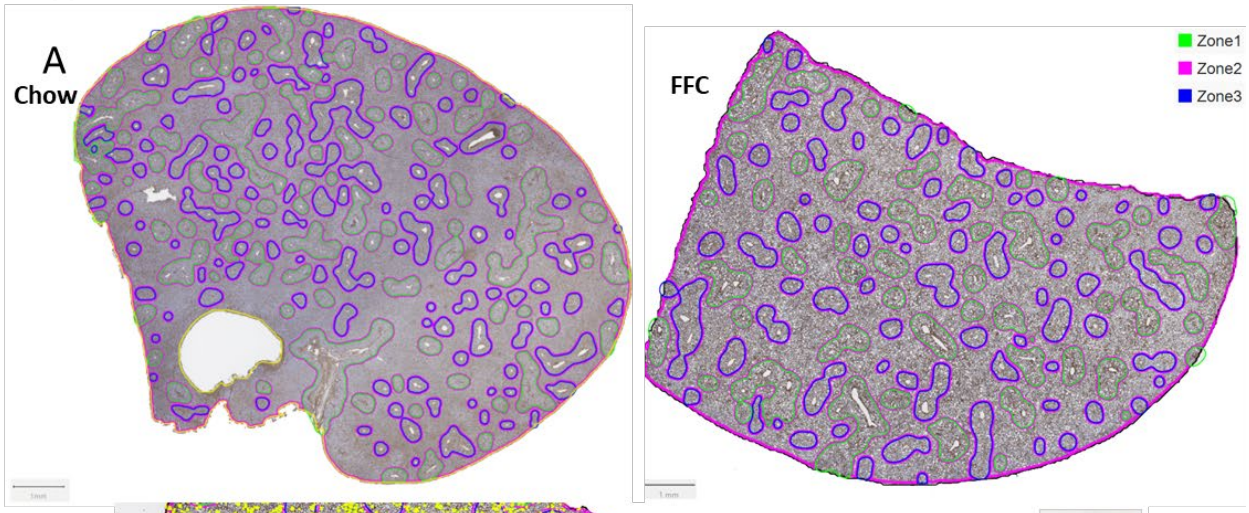

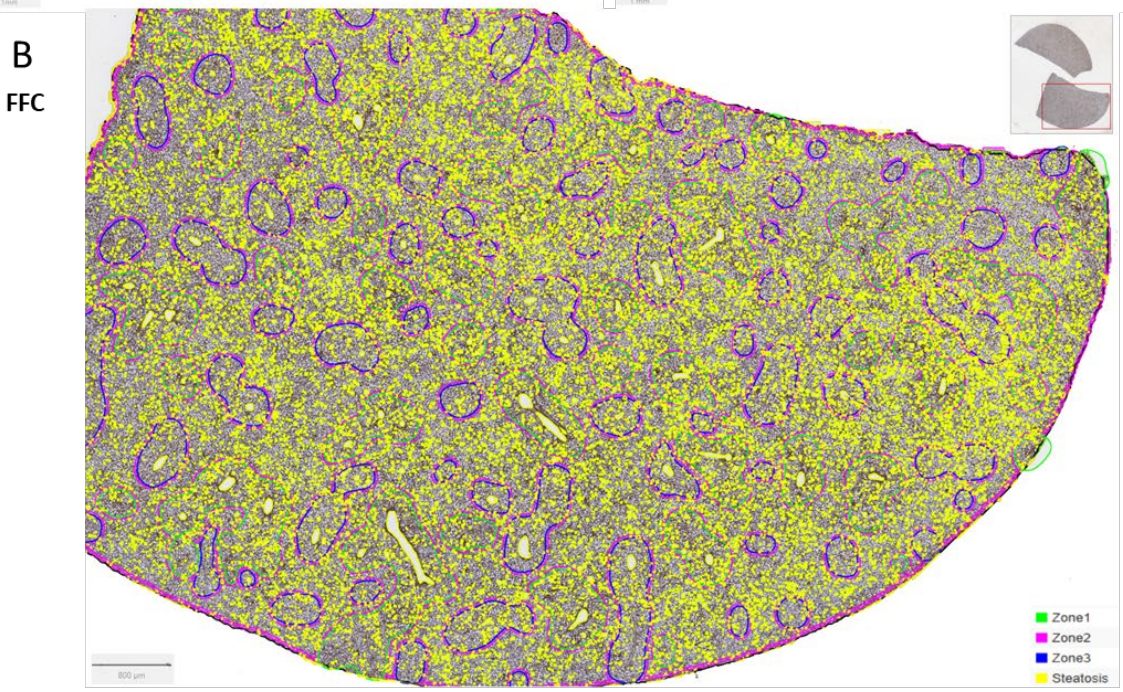

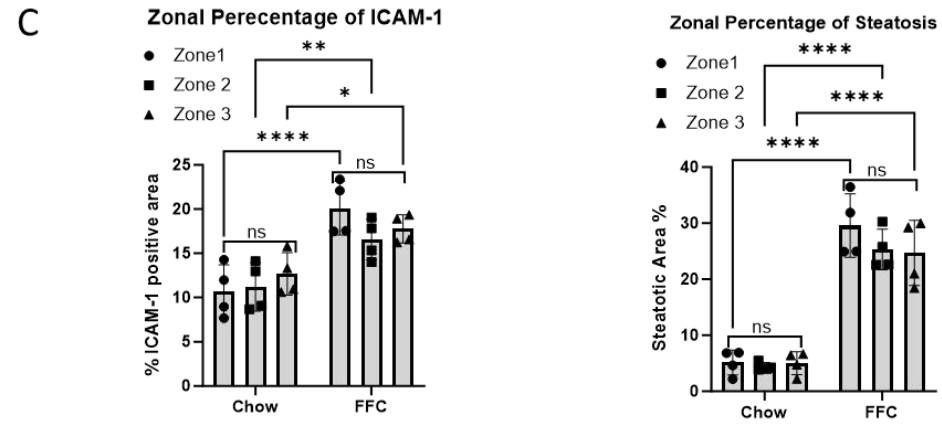

Fig. S2. Zonal distribution of lipotoxic endotheliopathy in vivo. *(*A) Images of digitized whole slides from mice with FFC diet-induced MASH and chow control; the slides were immunostained for ICAM-1, and zonal annotations were performed by the liver pathologist. (B) Image of a digitized whole slide from a mouse with FFC diet-induced MASH immunostained for ICAM-1 with zonal annotation and zonal steatosis representation using a machine learning algorithm. (C) Zonal percentages of ICAM-1 positive areas and-steatotic areas**.** (n=4 per group); bar graphs represent the mean ± SEM, *$p < 0.05$, **$p<0.01$, ****$p< 0.0001$, ns, non-significant (One-way ANOVA with Bonferroni's multiple comparison).

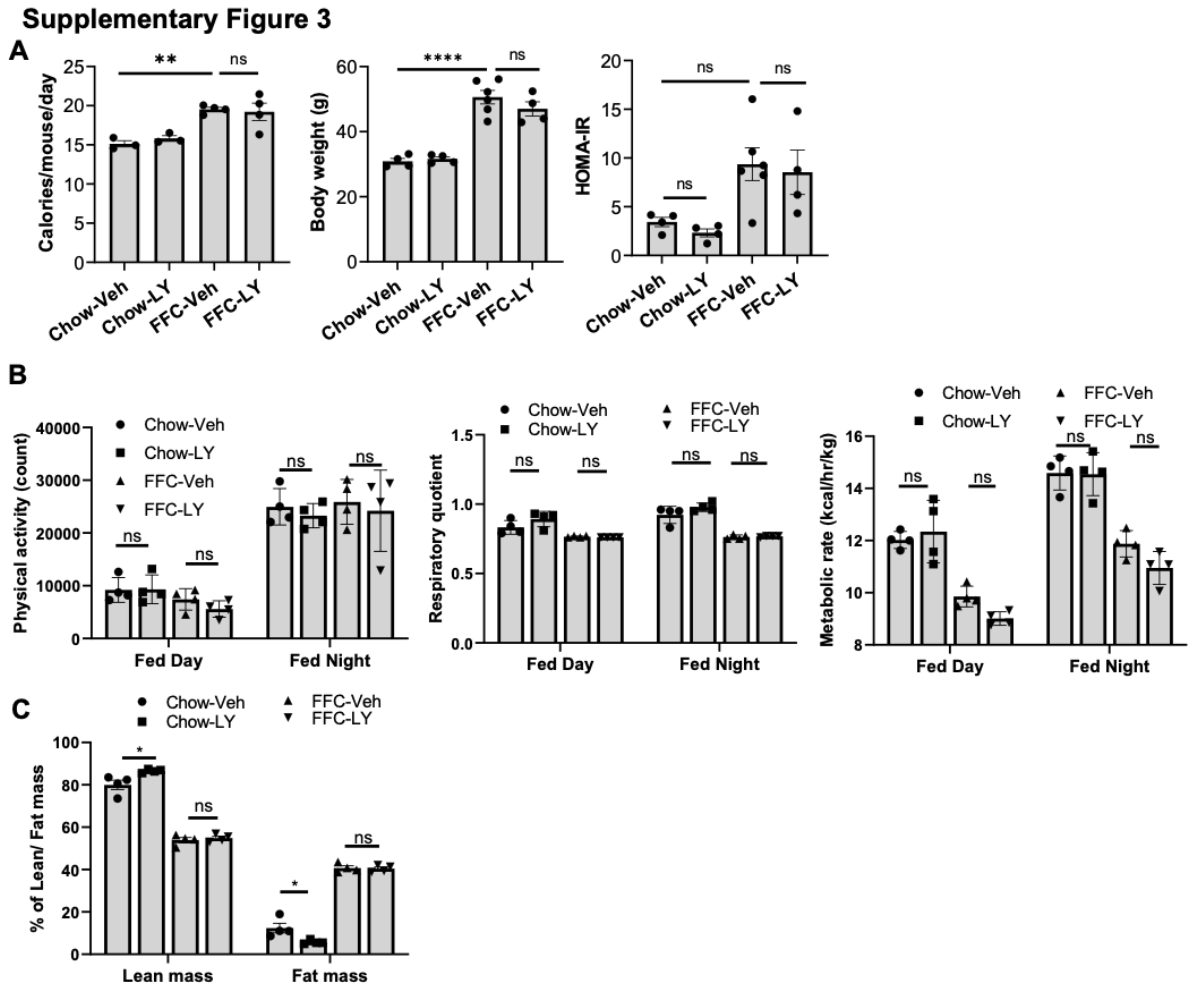

Fig. S3. LY2090314 was well-tolerated and did not affect insulin resistance or metabolic phenotypes in diet-induced murine MASH. Eight-week-old wild-type C57BL/6J mice were fed either a chow or FFC diet for 24 weeks to induce MASH and treated with either vehicle (Veh) or the GSK3 inhibitor LY2090314 (LY) for the last 4 weeks. (A) Daily caloric intake (left), body weight (middle), and HOMA-IR (right). (B) Physical activity, normalized respiratory quotient, and metabolic rate were assessed using the CLAMS study, and (C) lean versus fat mass body composition measured using Echo-MRI. Bar graphs represent mean ± SEM, *p < 0.05, **p<0.01, ****p< 0.0001, ns, nonsignificant (One-way ANOVA with Bonferroni's multiple comparison)

Supplementary Figure 4

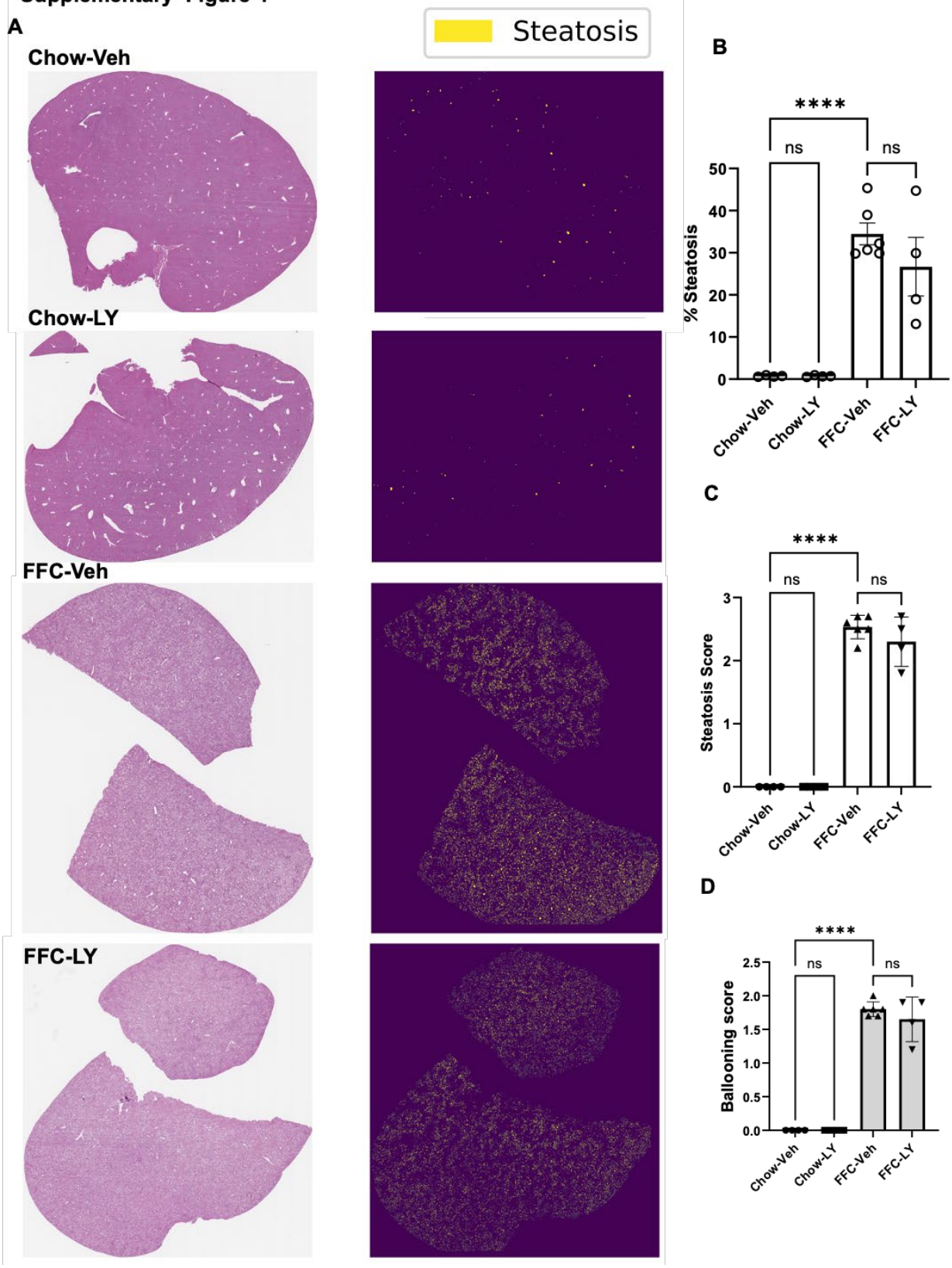

Fig. S4. LY treatment did not significantly reduce steatosis in MASH-treated mice. (A) Representative images of whole digitized H&E-stained slides and the corresponding steatotic areas from Chow- and FFC-fed mice treated with either vehicle or LY. (B) Automated quantification of steatosis percentage on digitized H&E-stained slides. (C) Steatosis scoring performed by estimating the steatotic area percentage in five fields per mouse and averaging (score 1 (6-33%), score 2 (33-66%), score 3 more than 66%)]. (D) Ballooning scores. (n=4-6 per group); bar graphs represent mean ± SEM, ****$p < 0.0001$, ns, non-significant (One-way ANOVA with Bonferroni's multiple comparison).

Supplementary Figure 5

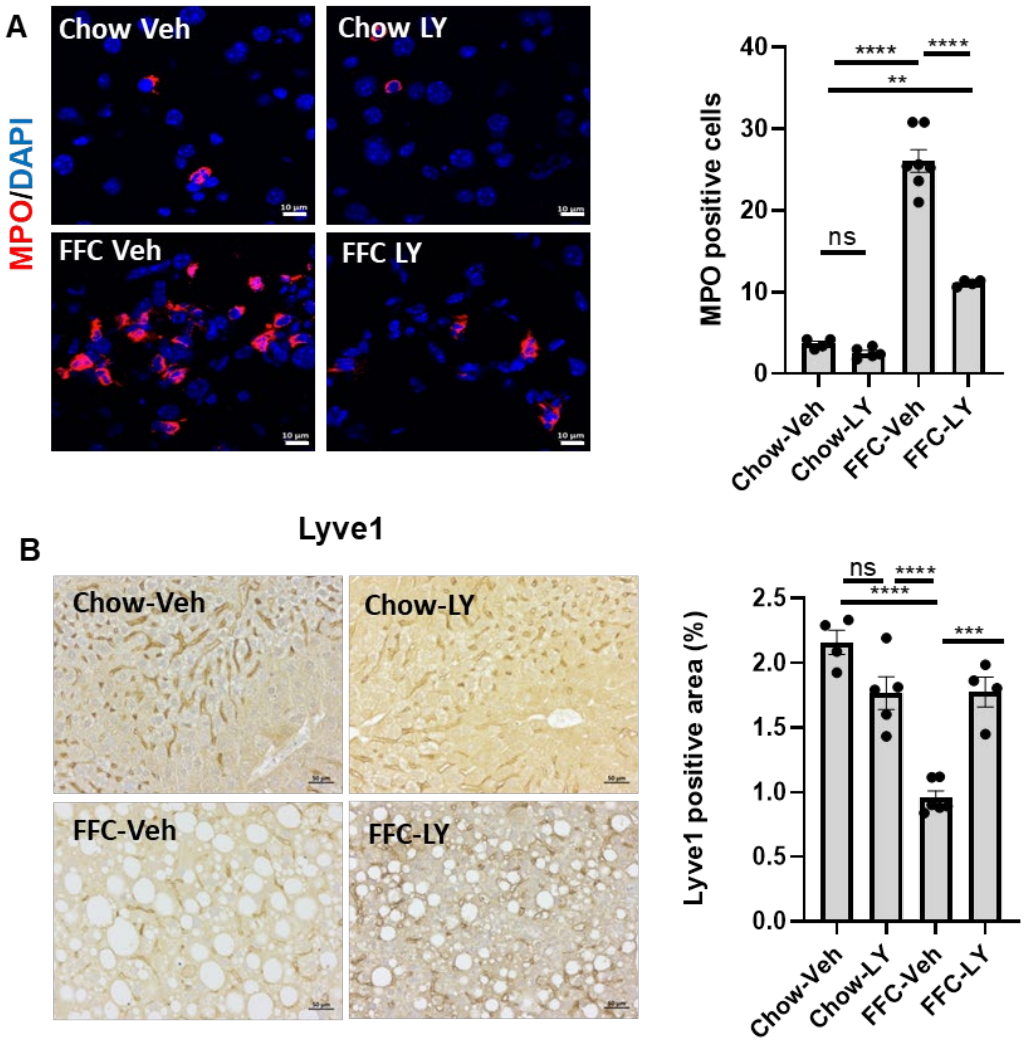

Fig. S5. LY treatment reduces hepatic neutrophil infiltration and restores LSEC differentiation in murine MASH. Representative images (A) for MPO immunofluorescence staining (red) and nuclei were stained with DAPI (blue). Images are shown at a 63x magnification. Scale bar: 10 µm. (B) Lyve 1 immunostaining of the liver sections (left). MPO and Lyve1 positive areas were quantified in 5 random 10x microscopic fields and averaged for each animal (right panel). Scale bar: 50 µm (n=4-6 per group) Bar graphs represent mean ± SEM, **p< 0.0001, ****p< 0.0001, ns, nonsignificant (One-way ANOVA with Bonferroni's multiple comparison).

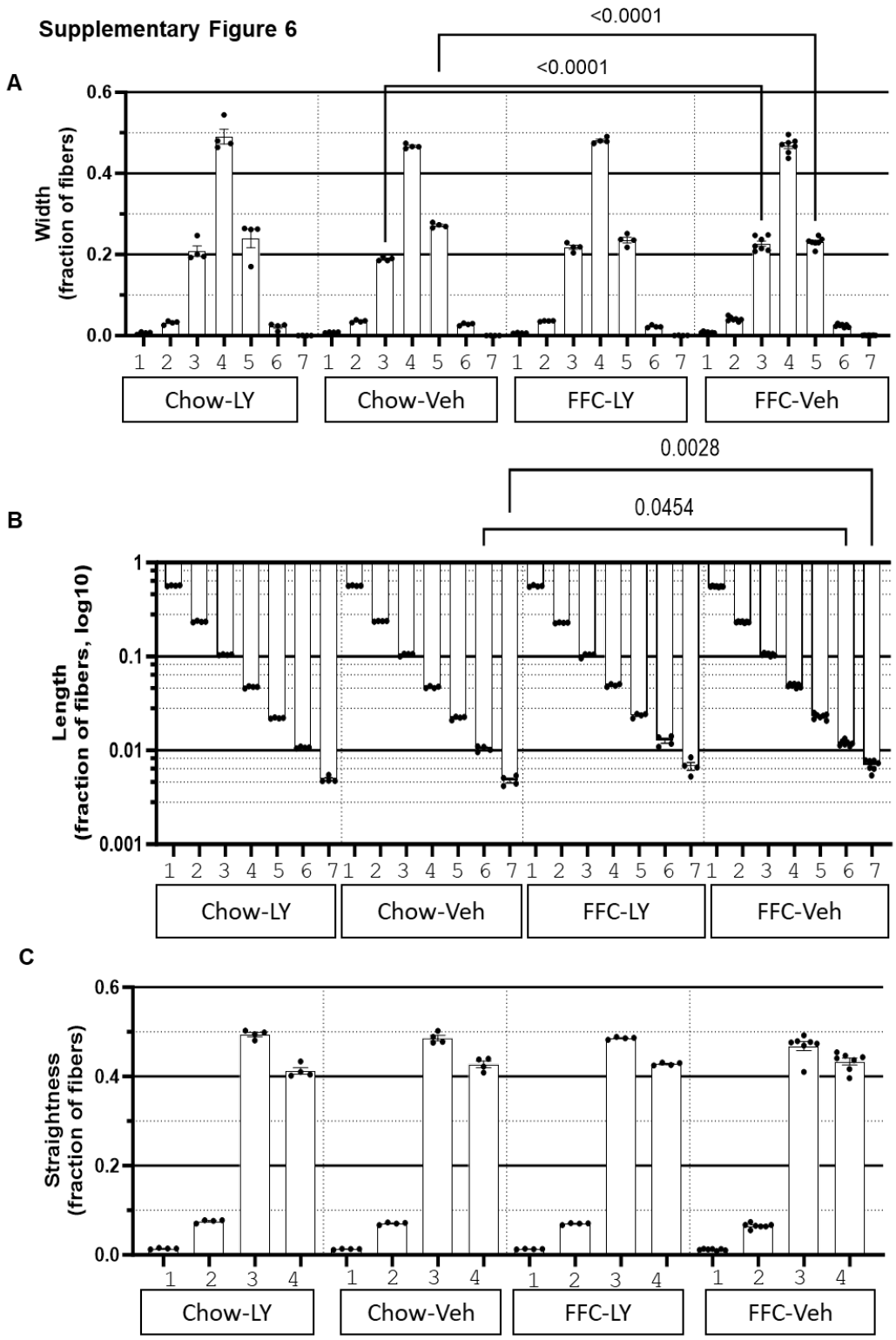

Fig. S6. Impact of the FFC diet on the fraction of hepatic collagen fiber width, length, and straightness. (A) Frequency histogram of collagen fiber width. The fiber widths were divided into

seven bins, from low (1) to high (7). Compared to regular chow, FFC increased the fraction of fibers in bin 3 and decreased the fraction in bin 5, indicating that FFC increased the prevalence of narrower fibers. Data are presented as mean ± SEM, n=4-7, p values by ANOVA. (B) Frequency histogram of the collagen fiber length. Fiber lengths were divided into seven bins from low (1) to high (7). FFC increased the fraction of longer fibers (bins 6 and 7). Data are presented as mean ± SEM, n=4-7, p values by ANOVA. (C) Frequency histogram of collagen fiber straightness. Fiber straightness was divided into four bins from low (1) to high (4). Neither FFC nor LY affected the distribution of fibers vs chow or FFC-Veh controls, respectively. Data are presented as mean ± SEM, n=4-7, p values by ANOVA.

Supplementary Figure 7

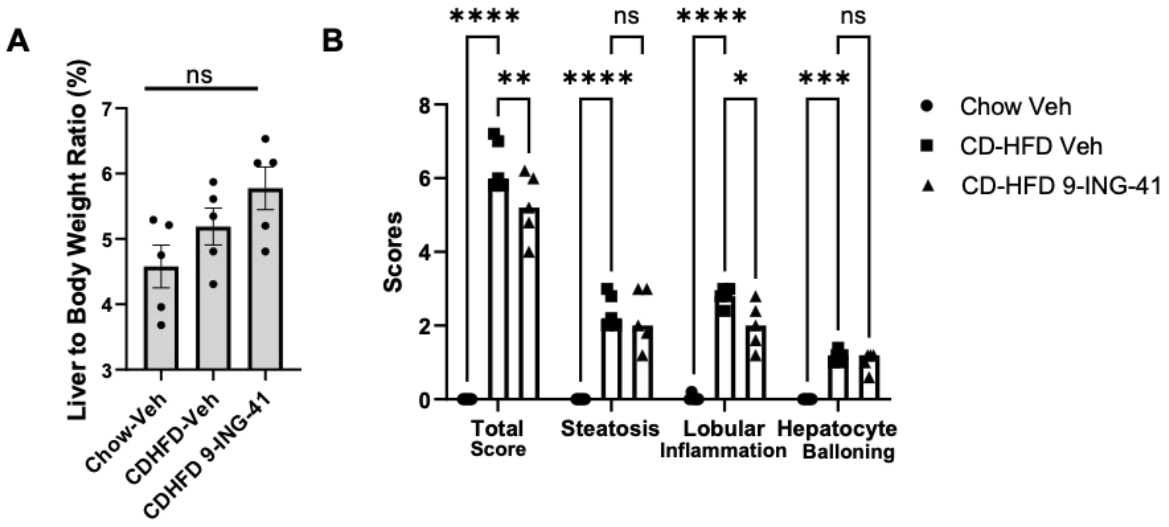

C

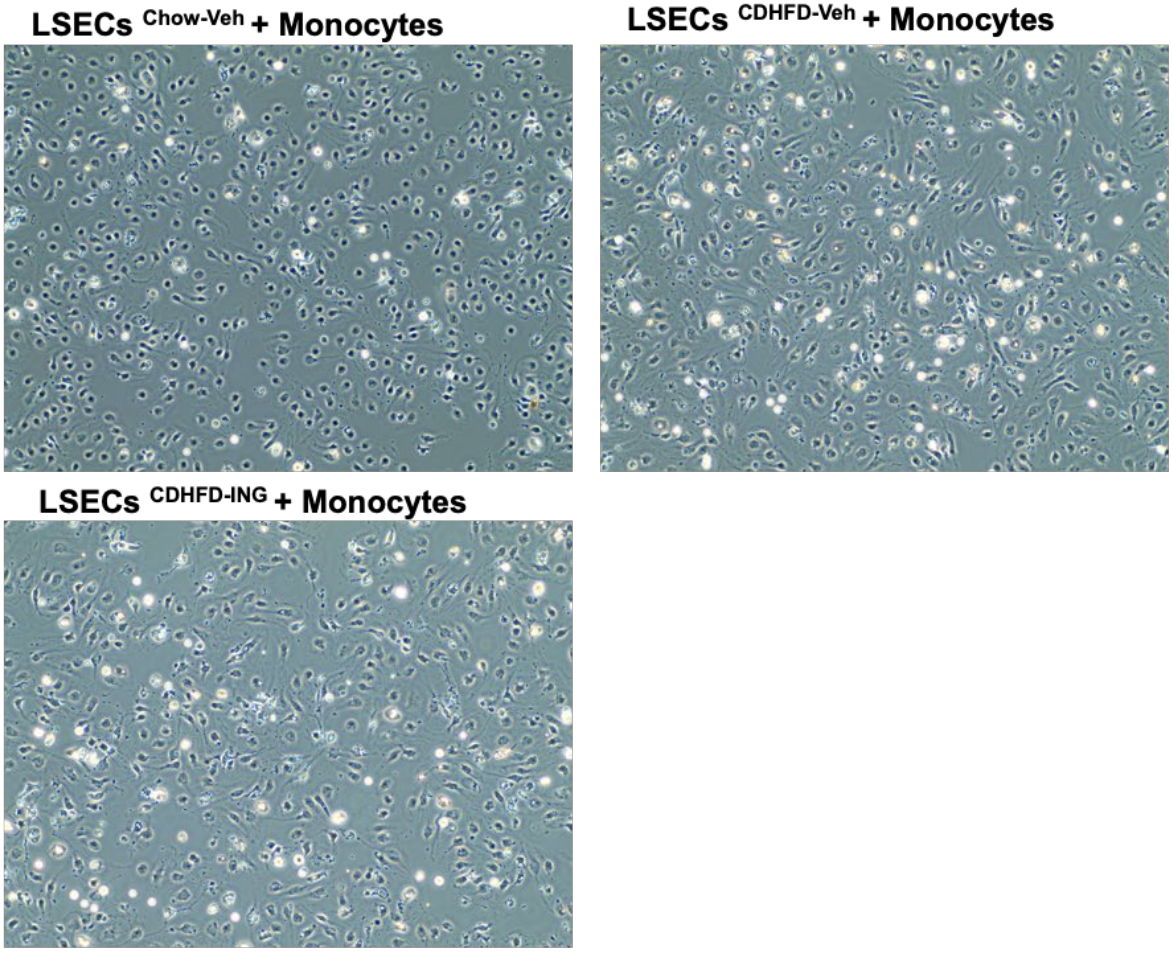

Fig. S7. 9-ING-41 treatment in MASH mice reduced lobular inflammation and monocyte adhesion to LSEC. Mice were fed chow or a CDHFD and treated with either vehicle or 9-ING-41 (A)**.** The liver-to-body weight ratio was also measured. (B) Steatosis, lobular inflammation, and hepatocyte ballooning were assessed using the NASH Clinical Research Network Scoring System (NAS). (C) Representative images of adherent bone marrow-derived monocytes to LSEC from control mice versus mice with diet-induced MASH treated with either vehicle or 9-ING-41 (n=5); bar graphs represent mean ± SEM, *p < 0.05, **p<0.01, ***p< 0.001, ****p< 0.0001, ns, non-significant (One-way ANOVA with Bonferroni's multiple comparison).

Supplementary Figure 8

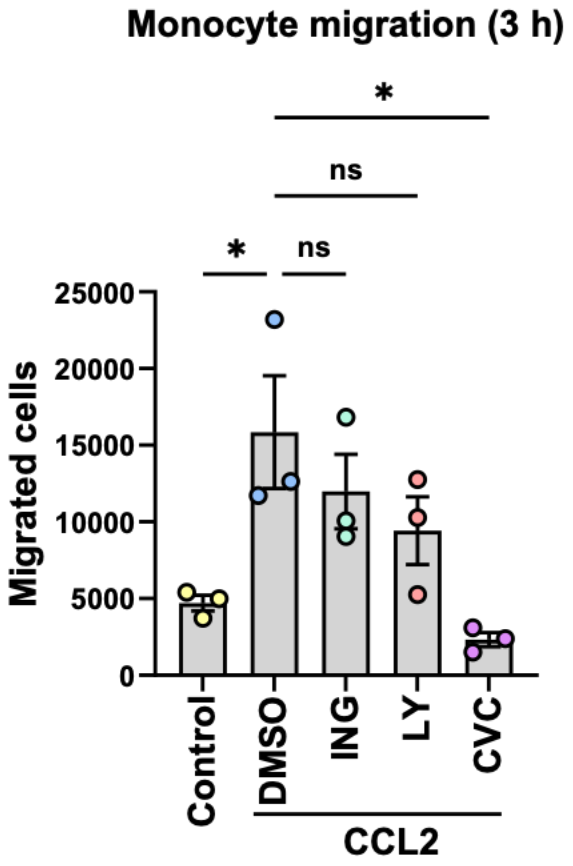

Fig. S8. Monocyte migration was not significantly altered by GSK3 inhibition, and monocytes were isolated from chow-fed mice and treated with the chemokine CCL2 (100 ng/ml) ± GSK3 inhibitors (LY 100 nM or ING 1 μM) or cenicriviroc (1 μM) in transwell inserts placed in a 24-well plate and allowed to migrate for 3 h. Migrated cells in the lower chamber were counted using an automated plate-based imaging cytometer (n=3 per group); bar graphs represent mean ± SEM, *$p < 0.05$, ns, non-significant (One-way ANOVA with Bonferroni's multiple comparison).

Supplementary Figure 9

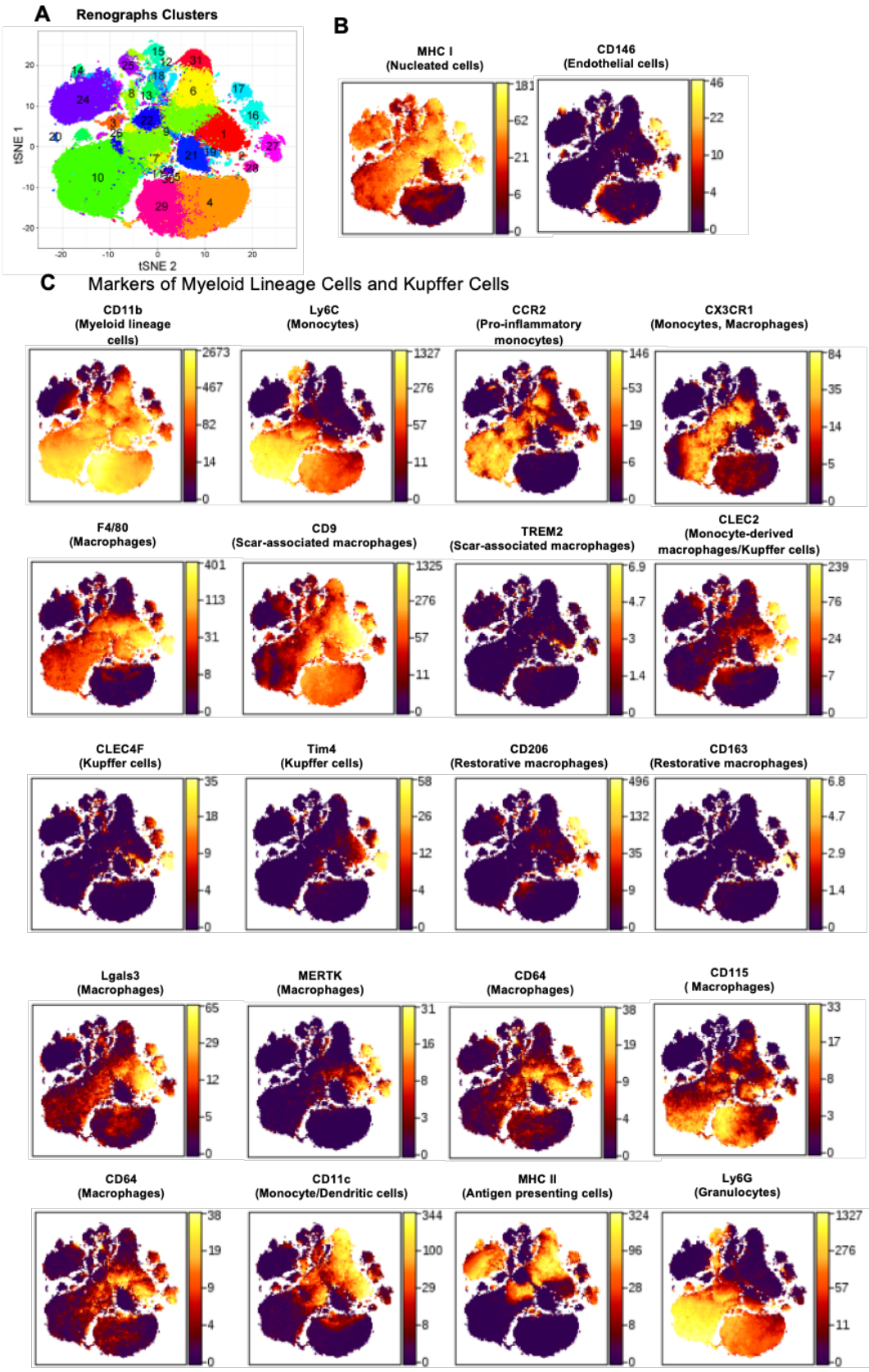

Supplementary Figure 9 (continued)

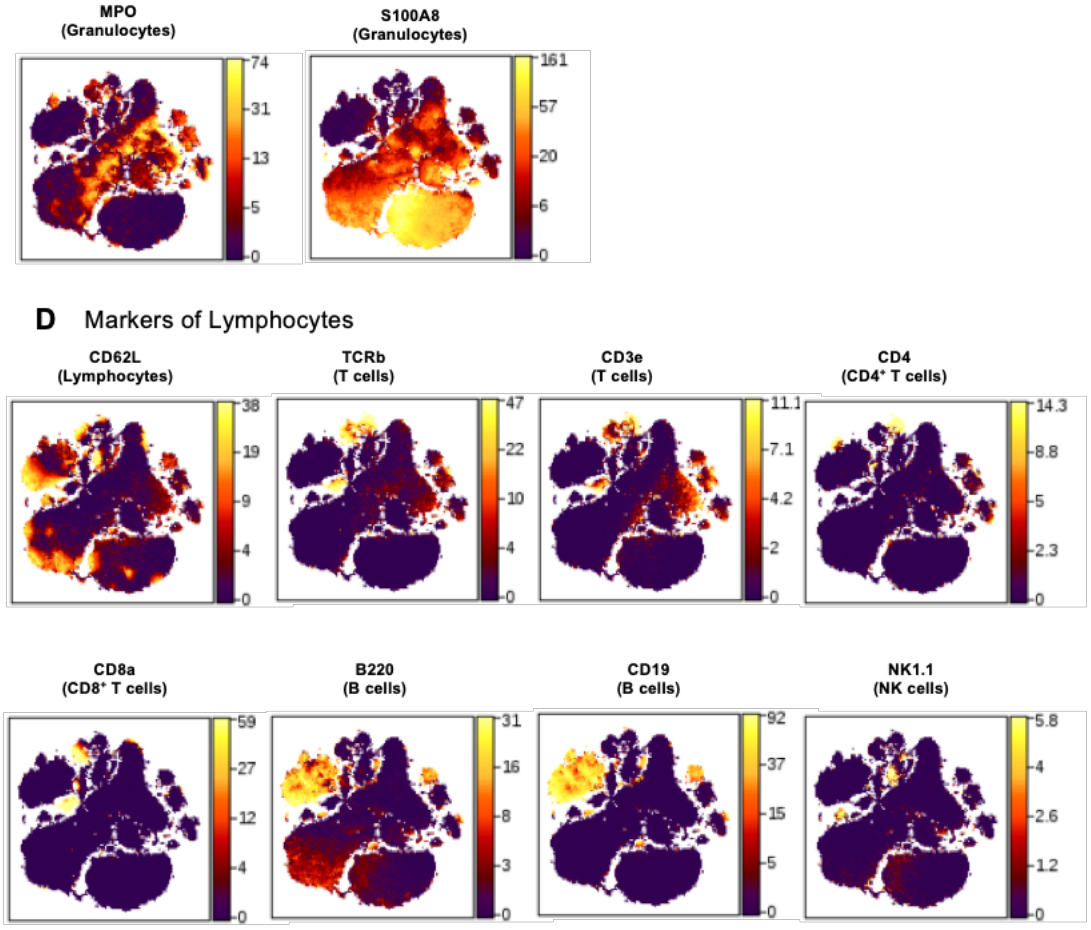

Fig. S9. Intrahepatic leukocyte (IHL) profiling by mass cytometry by time-of-flight (CyTOF). CyTOF was performed on IHL of control vehicle-treated chow-fed mice, and CDHFD-fed mice treated with either 9-ING-41 or vehicle. Thrirty-one unique clusters were defined using a panel of 32 different cell surface markers and two cytosolic markers (shown in Supplementary Table 1-2). (A) t-distributed stochastic neighbor embedding (tSNE) plot generated using the Rphenograph clustering algorithm (identical to Figure 7A). (B) tSNE plots depicting the density of MHC-I, and CD146 positive cells in each cluster. (C and D) tSNE plots depicting cell surface marker densities for (C) myeloid-lineage cells and Kupffer cells and (D) lymphocytes in each cluster.

Supplementary Figure 10

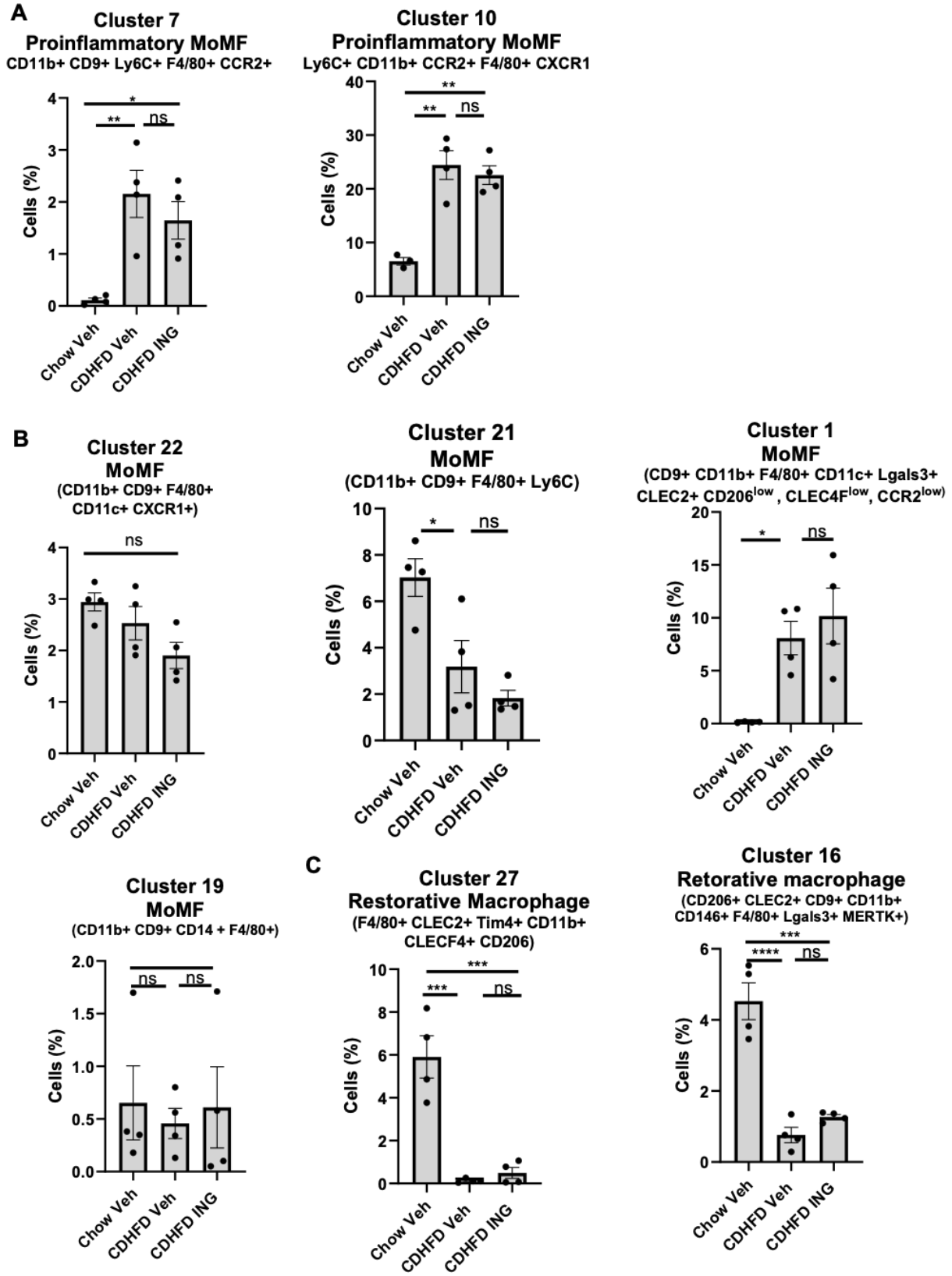

Supplementary Figure 10 (Continued)

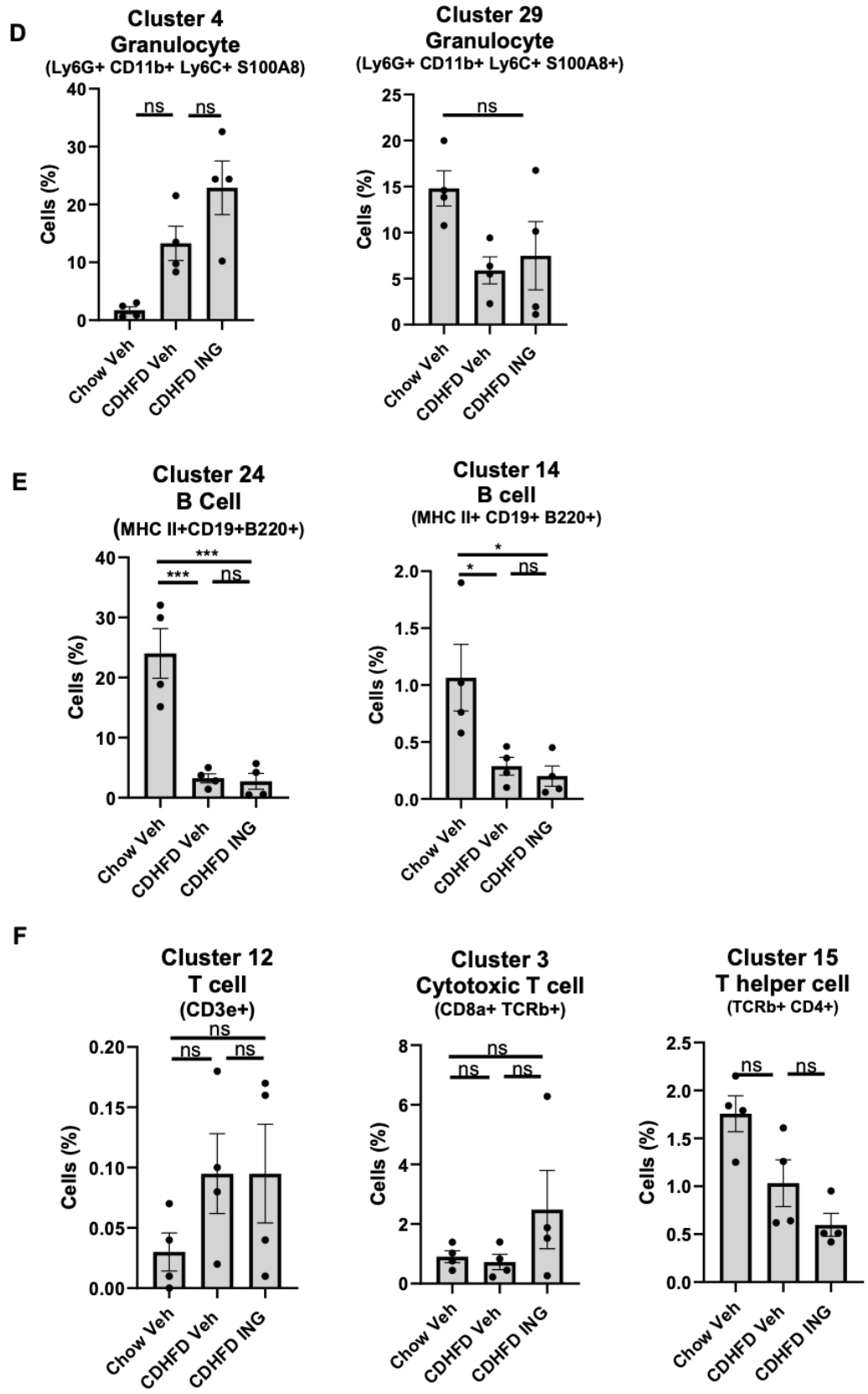

Fig. S10. 9-ING-41 treatment of CDHFD-fed mice does not significantly alter the granulocyte, T cell, or B cell populations. The proportion of cells in specific clusters was quantified for each experimental group. (A) Clusters 7 and 10 were categorized into proinflammatory monocyte-derived macrophages (MoMF), (B) Clusters 22, 21, 1 and 19 into monocyte-derived macrophages (MoMF), (C) Clusters 27 and 16 into restorative MoMF, (D) Clusters 4 and 29 into granulocytes, and (E) Clusters 24 and 14 into B cells, (F) Cluster 12 into T cells, Cluster 3 into cytotoxic T cells, Cluster 15 into T helper cell (n=4 per group); bar graphs represent mean ± SEM, *$p < 0.05$, **$p<0.01$,***$p<0.001$,****$p<0.0001$ ns, nonsignificant (One-way ANOVA with Bonferroni's multiple comparison).

Supplementary tables

Table S1

No.	Sp.	Label	Target	Clone	Company	Catalog Number
1	Ms	089Y	CD45	30-F11	Fluidigm	3089005B
2	Ms	106Cd	CD146	ME-9F1	Biolegend	134702
3	Ms	112Cd	CD4	RM4-5	Biolegend	100561
4	Ms	116Cd	MPO	EPR20257	Abcam	ab221847
5	Ms	141Pr	Lgals3	202213	R&D Systems	MAB1197
6	Ms	142Nd	CD11c	N418	Fluidigm	3142003B
7	Ms	143Nd	TCRb	H57-597	Fluidigm	3143010B
8	Ms	144Nd	MHC Class I	28-14-8	Fluidigm	3144016B
9	Ms	145Nd	CLEC-2 (CLEC1B)	17D9/CLEC-2	Biolegend	146102
10	Ms	147Sm	CD9	MZ3	Biolegend	124802
11	Ms	148Nd	CXCR2	SA044G4	Biolegend	149302
12	Ms	149Sm	Tim4	RMT4-54	BioLegend	130002
13	Ms	151Eu	CD206 (MMR)	C068C2	BioLegend	141702
14	Ms	152Sm	CD3e	145-2C11	Fluidigm	3152004B
15	Ms	153Eu	CLEC4F/CLECSF13	poly Goat	R&D	AF2784
16	Ms	154Sm	CD62L (L-selectin)	MEL-14	BioLegend	
17	Ms	155Gd	MERTK	108928	R&D Systems	MAB5912
18	Ms	156Gd	CCR2	475301	R&D Systems	MAB55381
19	Ms	159Tb	F4/80	BM8	Fluidigm	3159009B
20	Ms	160Gd	CD64	290322	R&D Systems	MAB20741
21	Ms	161Dy	Ly6G	1A8	BioLegend	127637
22	Ms	164Dy	CX3CR1	SA011F11	Fluidigm	3164023B
23	Ms	165Ho	CD14	Sa14-2	BioLegend	123321
24	Ms	166Er	CD19	6D5	Fluidigm	3166015B
25	Ms	167Er	TREM2	237920	R&D	MAB17291
26	Ms	168Er	CD8a	53-6.7	Fluidigm	3168003B
27	Ms	169Tm	CD163	S15049	Biolegend	155302
28	Ms	170Er	CD161 (NK1.1)	PK136	Fluidigm	3170002B
29	Ms	172Yb	CD11b (Mac-1)	M1/70	Fluidigm	3172012B
30	Ms	173Yb	S100A8	63N13G5	NOVUS	NBP2-25273
31	Ms	174Yb	CD115/CSF1R	AFS98	BioLegend	135521
32	Ms	175Lu	Ly6C	HK1.4	BioLegend	128039
33	Ms	176Yb	CD45R (B220)	RA3-6B2	Fluidigm	3176002B
34	Ms	209Bi	I-A/I-E (MHC II)	M5/114.15.2	BioLegend	107637

Table S2

Antibody panel of 33 markers

Macrophages F4/80, CD64, Tim4, MERTK, CD206, CD163, Lgals3, CD115, CD14, CLEC2, CLEC4F, TREM2, MHCI	**Pan-leukocyte** CD45	**Dendritic cells** CD11c, MHCII
	Monocytes Ly6C, CCR2, CX3CR1, CD11b, CD14	**NK cells** NK1.1
		B cells B220, CD19
Neutrophils CD11b, Ly6G, **MPO, S100A8**	**T cells** CD3e, CD8a, TCRb, CD4	**LSEC** CD146

Table S3

Annotated Clusters Based on Surface Markers

Cluster number	Positive Surface Markers	Annotation
1	CD9+, CD11b+, F4/80+, CD11c+, Lgal3+, CXCR2+, CLEC2+ ,CD206^{low}, CLEC4F^{low}, CCR2^{low}	Monocyte derived Macrophage (MoMF) (CD11b+ F4/80+)
3	CD8a+, TCRb+	Cytotoxic T cells (CD8a+, TCRb+)
4	Ly6G+, CD11b+, Ly6C+	Granulocyte (Ly6G+)
6	CD11b+, CD11c+, MHCII+, CCR2+	Monocyte derived Dendritic cells (MoDC) (CD11b+ MHC II+ CD11c+)
7	CD11b+, CD9+, Ly6C+, F4/80+, CD11c+, CCR2+, CX3CR1+	Proinflammatory MoMF (CD11b+, F4/80+,CCR2+)
9	CD11b+, CD9+, F4/80+, CCR2+, CX3CR1+	Proinflammatory MoMF (CD11b+, F4/80+,CCR2+)
10	Ly6c+, CD11b+, CCR2+, CX3CR1+	Proinflammatory MoMF (CD11b+, F4/80+,CCR2+)
12	CD3e+	T cell (CD3e+)
14	MHCII+, CD19+, B220+	B cells (CD19+, B220+)
15	CD4+, TCRb+	T helper (CD4+, TCRb+)
19	CD11b+ CD9+ CD14 + F4/80+	MoMF (CD11b+ F4/80+)
21	CD11b+ CD9+ F4/80+ Ly6C	MoMF (CD11b+ F4/80+)
22	CD11b+ CD9+ F4/80+ CD11c+ CXCR1+	MoMF (CD11b+ F4/80+)
24	MHCII+, CD19+, B220+, CDL62+	B cells (CD19+, B220+)
29	Ly6G+, CD11b+, Ly6C+	Granulocyte (Ly6G+)
27	F4/80+ CLEC2+ Tim4+ CD11b+ CLECF4+ CD206+	Restorative Macrophage (F4/80+ CLECF4+ CD206+)
31	CD11b+, MHCII+, CD11c+, CCR2+	MoDC (CD11b+ MHC II+ CD11c+)

Table S4

PCR primers:

Name	**Sequence**
Mouse *Ccr2* Forward Primer	ATCCACGGCATACTATCAACATC
Mouse *Ccr2* Reverse Primer	CAAGGCTCACCATCATCGTAG
18S Forward Primer	CGCTTCCTTACCTGGTTGAT
18S Reverse Primer	GAGCGACCAAAGGAACCATA
Mouse *Col1a1* Forward Primer	GCTCCTCTTAGGGGCCACT
Mouse *Col1a1* Reverse Primer	CCACGTCTCACCATTGGGG
Human *CXCL2* Forward Primer	CATCGAAAAGATGCTGAAAAATG
Human *CXCL2* Reverse Primer	TTCAGGAACAGCCACCAATA
Mouse *Cxcl2* Forward Primer	CCAACCACCAGGCTACAGG
Mouse *Cxcl2* Reverse Primer	GCGTCACACTCAAGCTCTG
Human *ICAM-1* Forward Primer	TATAAAGGATCACGCGCCCC
Human *ICAM-1* Reverse Primer	GACTCACCTGGGAACAGAGC
Human *GSK3b* Forward Primer	GGCAGCATGAAAGTTAGCAGA
Human *GSK3b* Reverse Primer	GGCGACCAGTTCTCCTGAATC
Mouse *Col1α1* Forward Primer	GCTCCTCTTAGGGGCCACT
Mouse *Col1α1* Reverse Primer	CCACGTCTCACCATTGGGG
Mouse *Acta2* Forward Primer	GTCCCAGACATCAGGGAGTAA
Mouse *Acta2* Reverse Primer	TCGGATACTTCAGCGTCAGGA

Supplementary references

[1] Furuta K, Guo Q, Pavelko KD, et al. Lipid-induced endothelial vascular cell adhesion molecule 1 promotes nonalcoholic steatohepatitis pathogenesis. J Clin Invest 2021;131.
[2] Guo Q, Furuta K**,** Aly A, et al. Isolation and Characterization of Mouse Primary Liver Sinusoidal Endothelial Cells. J Vis Exp 2021.
[3] Huebert RC, Jagavelu K, Liebl AF, et al. Immortalized liver endothelial cells: a cell culture model for studies of motility and angiogenesis. Lab Invest 2010;90:1770-1781.
[4] Muller WA, Luscinskas FW. Assays of transendothelial migration in vitro. Methods Enzymol 2008;443:155-176.
[5] Sullivan DP, Dalal PJ, Jaulin F, et al. Endothelial IQGAP1 regulates leukocyte transmigration by directing the LBRC to the site of diapedesis. J Exp Med 2019;216:2582-2601.
[6] Krishnan A, Abdullah TS, Mounajjed T, et al. A longitudinal study of whole body, tissue, and cellular physiology in a mouse model of fibrosing NASH with high fidelity to the human condition. Am J Physiol Gastrointest Liver Physiol 2017;312:G666-g680.
[7] Ibrahim SH, Hirsova P, Tomita K, et al. Mixed lineage kinase 3 mediates release of C-X-C motif ligand 10-bearing chemotactic extracellular vesicles from lipotoxic hepatocytes. Hepatology 2016;63:731-744.
[8] **Guo Q, Furuta K**, Lucien F, et al. Integrin beta1-enriched extracellular vesicles mediate monocyte adhesion and promote liver inflammation in murine NASH. J Hepatol 2019;71:1193-1205.
[9] Atkinson JM, Rank KB, Zeng Y, et al. Activating the Wnt/beta-Catenin Pathway for the Treatment of Melanoma--Application of LY2090314, a Novel Selective Inhibitor of Glycogen Synthase Kinase-3. PLoS One 2015;10:e0125028.
[10] Zhao P, Sun X, Chaggan C, et al. An AMPK-caspase-6 axis controls liver damage in nonalcoholic steatohepatitis. Science (New York, NY) 2020;367:652-660.
[11] Jeffers A, Qin W, Owens S, et al. Glycogen Synthase Kinase-3beta Inhibition with 9-ING-41 Attenuates the Progression of Pulmonary Fibrosis. Sci Rep 2019;9:18925.
[12] Tomita K, Kohli R, MacLaurin BL, et al. Mixed-lineage kinase 3 pharmacological inhibition attenuates murine nonalcoholic steatohepatitis. JCI Insight 2017;2.
[13] Kleiner DE, Brunt EM, Van Natta M, et al. Design and validation of a histological scoring system for nonalcoholic fatty liver disease. Hepatology 2005;41:1313-1321.
[14] Wegner KA, Keikhosravi A, Eliceiri KW, et al. Fluorescence of Picrosirius Red Multiplexed With Immunohistochemistry for the Quantitative Assessment of Collagen in Tissue Sections. J Histochem Cytochem 2017;65:479-490.
[15] Bredfeldt JS, Liu Y, Pehlke CA, et al. Computational segmentation of collagen fibers from second-harmonic generation images of breast cancer. J Biomed Opt 2014;19:16007.
[16] Bradski G. The OpenCV library. Dr Dobbs J 2000;25:120-+.
[17] Li J, Van Vranken JG, Pontano Vaites L, et al. TMTpro reagents: a set of isobaric labeling mass tags enables simultaneous proteome-wide measurements across 16 samples. Nat Methods 2020;17:399-404.
[18] Perez-Riverol Y, Bai J, Bandla C, et al. The PRIDE database resources in 2022: a hub for mass spectrometry-based proteomics evidences. Nucleic Acids Res 2022;50:D543-D552.
[19] Chen H, Lau MC, Wong MT, et al. Cytofkit: A Bioconductor Package for an Integrated Mass Cytometry Data Analysis Pipeline. PLoS Comput Biol 2016;12:e1005112.